

Effects of Magnetovolume and Spin-Orbit Coupling in Ferromagnetic Cubic Perovskite BaRuO₃

Young-Joon Song¹ and Kwan-Woo Lee^{1,2*}

¹Department of Applied Physics, Graduate School, Korea University, Sejong 339-700, Korea

²Department of Display and Semiconductor Physics, Korea University, Sejong 339-700, Korea
(Dated: September 30, 2018)

BaRuO₃ having five different crystal structures has been synthesized by varying the pressure while sintering. Contrary to the other phases being nonmagnetic, the cubic perovskite phase synthesized recently shows itinerant ferromagnetic character. We investigated this ferromagnetic BaRuO₃ using first principles calculations. A few van Hove singularities appear around the Fermi energy, causing unusually high magnetovolume effects of $\Delta M/\Delta a \approx 4.3 \mu_B/\text{\AA}$ as well as the Stoner instability [$IN(0) \approx 1.2$]. At the optimized lattice parameter a , the magnetic moment M is $1.01 \mu_B$ in the local spin density approximation. When spin-orbit coupling is included, the topology of some Fermi surfaces is altered, and the moment is reduced by 10 % to a value very close to the experimentally observed value of $\sim 0.8 \mu_B$. Our results indicate that the ferromagnetism is induced by the Stoner instability, but the combined effects of magnetovolume and spin-orbit coupling determine the net moment. In addition, we briefly discuss the results of the tight-binding Wannier function technique.

PACS numbers: 71.20.Be, 71.20.Dg, 75.50.Cc, 75.80.+q

Keywords: Electronic structure, BaRuO₃, Spin-orbit coupling

I. INTRODUCTION

Ruthenates, which possess formally tetravalent Ru ions of $4d^4$, show interesting properties: unconventional superconductivity in Sr₂RuO₄,[1] the metal-insulator transition in La₂Ru₂O₇ and Li₂RuO₃,[2, 3] metamagnetism in Sr₃Ru₂O₇,[4] and complicated magnetic behaviors in double pyrochlore RE₂Ru₂O₇ (RE=rare earth element).[5] In particular, the Ru-based perovskites ARuO₃ (A=alkaline-earth elements and Pb) have been studied extensively for several decades due to their atypical and controversial electronic and magnetic behaviors.[6–12] SrRuO₃ is a metallic ferromagnet with $T_C=160$ K and an experimentally observed moment of $\sim 1.6 \mu_B$, whereas CaRuO₃ is a nonmagnetic metal.[13, 14] PbRuO₃ seems to exhibit incipient magnetism, but whether this system is a metal or an insulator at low T is still under debate.[15, 16] The crystal structure of BaRuO₃ depends strongly on the temperature and pressure during synthesis,[17] whereas the other compounds are orthorhombic. Depending on the amount of corner- and face-sharing RuO₆, the structures of BaRuO₃ are categorized as the four-, six-, and ten-layered hexagonal phases (4H, 6H, and 10H, respectively), in addition to the nine-layered rhombohedral phase (9R).[18–22] As discussed both theoretically and experimentally,[12, 18, 23] the 10H and 9R phases seem to be semi-metallic, whereas the rest are nonmagnetic metals. Early in 2008, Jin *et al.* synthesized the cubic phase using the technique of high T (~ 1000 °C) and high P (~ 18 GPa).[17]

In this research, we will focus on the cubic phase, which

shows ferromagnetic behavior with $T_C=60$ K.[17] On the basis of resistivity measurements, which show a sharp peak in the T-derivation of the resistivity at T_C , Jin *et al.* suggested simple metallic characteristics in the high T regime, but Fermi liquid behavior in the low T regime. The effective magnetic moment is $2.6 \mu_B$, close to the value for $S=1$. However, the saturated moment of $0.8 \mu_B$ is significantly less than the value corresponding to $S=1$, implying atypical magnetic behaviors. Moreover, when pressure is applied, T_C decreases, reaching 50 K at $P=3$ GPa.

The elastic properties and pressure effects have been theoretically investigated to some extent,[24, 25] but no detailed studies of the magnetic and electric properties of this cubic phase have been reported yet. Thus, we will address the magnetic properties of this system through first principles calculations, including the local spin density approximation (LSDA), the LSDA plus spin-orbit coupling (LSDA+SOC), fixed spin moment (FSM), and tight-binding Wannier analysis.

II. STRUCTURE AND METHOD OF CALCULATION

First, we optimized the lattice parameter a in the cubic phase. LSDA calculations lead to our optimized $a=3.938$ Å. This value is about 1.7% smaller than the experimentally observed value at room temperature.[17] We used the optimized lattice parameter in our calculations, since the total moment at the optimized a is close to the experimental value, as discussed in the next section.

Our calculations were carried out with LSDA and LSDA+SOC implemented in the all-electron full-potential code WIEN2k.[26] The basis size was determined by $R_{mt}K_{max}=7$ and APW sphere radii of 2.5

*Electronic address: mckwan@korea.ac.kr

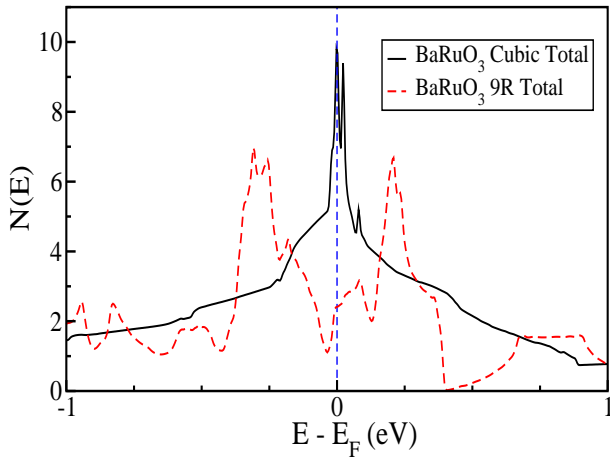


FIG. 1: (Color online) Comparison of nonmagnetic total densities of states (DOSs) per formula unit between cubic and 9R BaRuO₃. For the cubic phase, the optimized lattice parameter was used. In the cubic phase, two sharp peaks appear around the Fermi energy E_F , implying magnetic instability. The vertical dashed line indicates E_F , which is set to zero.

for Ba, 2.0 for Ru, and 1.7 for O. The Brillouin zone was sampled with $14 \times 14 \times 14$ k -mesh. For both the LSDA+SOC and FSM calculations,[27] a much denser k -mesh of $20 \times 20 \times 20$ was used. The lattice parameter was relaxed until the forces were smaller than 2 mRy/a.u. Furthermore, the all-electron full-potential local-orbital code FPLO was used for the tight-binding Wannier function analysis.[28]

III. RESULTS

Figure 1 shows the overlapped total densities of states (DOSs) between the nonmagnetic 9R and cubic phases between -1 and 1 eV. The DOS of the cubic phase is five times larger than that of 9R due to sharp peaks at E_F and 30 meV, suggesting strong magnetic instability.

Using LSDA, we calculated the change in the total magnetic moment while varying a from the experimental value to a value slightly smaller than the optimized one. As shown in the inset of Fig. 2, the magnetic moment decreases linearly with a slope of $\Delta M / \Delta a \approx 4.3 \mu_B / \text{\AA}$, indicating strong magnetovolume effects. This value is much larger than that of $\sim 1 \mu_B / \text{\AA}$ in the Invar systems $A\text{Fe}_2$ ($A=\text{Y, Zr, Hf, and Lu}$).[29]

Fixed spin moment studies. To investigate these behaviors, FSM calculations were conducted. Plots of energy versus total magnetic moment M for varying values of the lattice parameter a are shown in Fig. 2. The difference in energy between the $M=0$ and ferromagnetic (FM) ground states decreases monotonically from ~ 32 meV at $a=4.01 \text{ \AA}$ to 17 meV at 3.93 \AA . The curves are fitted well by $E(M) - E(0) \approx -\alpha M^2 + \beta M^4$ with constants α and β in low M regime. For the bare susceptibility $\chi_0 = 2\mu_B^2 N(0)$, the Stoner-enhanced susceptibility

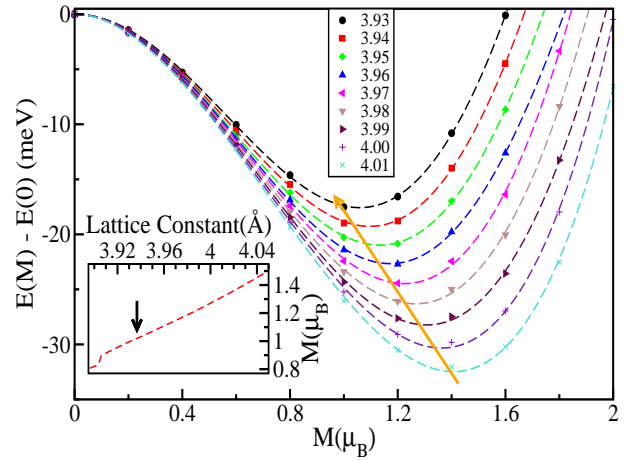


FIG. 2: (Color online) FSM calculations in the cubic phase, while changing the lattice parameter a (in units of \AA). $E(0)$ denotes the energy of the nonmagnetic state for a . The arrow roughly connects the minimum energy states. *Inset:* Change in total magnetic moment M with respect to a in the FM calculations. The arrow indicates the value at the optimized a . A discontinuity occurs at $a \sim 3.91 \text{ \AA}$, since E_F pins a van Hove singularity in the spin up channel (see below).

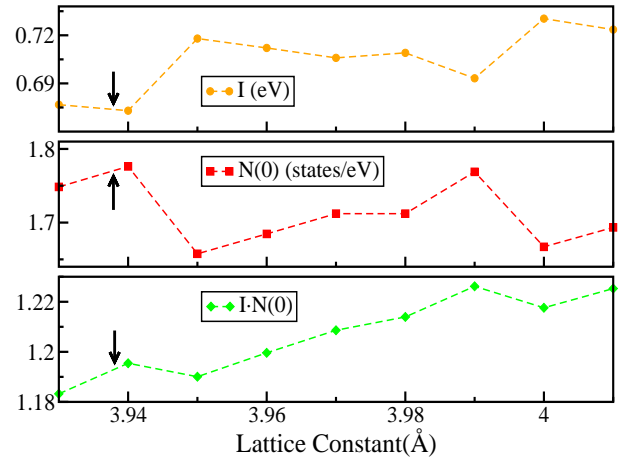


FIG. 3: (Color online) Change in Stoner parameter I (top), DOS $N(0)$ per single spin at E_F (middle), and $IN(0)$ (bottom) versus lattice parameter in the cubic BaRuO₃. Roughly, $IN(0)$ decreases linearly as the lattice parameter decreases.

is given by $\chi = \chi_0 / [1 - N(0)I]$, where $N(0)$ is the single-spin DOS at E_F . In low M regime, $\alpha = \frac{1}{2}\chi^{-1}$. The top panel of Fig. 3 displays the obtained Stoner parameters $I \approx 0.70(\pm 0.02) \text{ eV}$ for each a . As a changes, the DOS at E_F fluctuates substantially owing to van Hove singularities (vHSs) near E_F (see below), as given in the middle panel of Fig. 3. $IN(0)$ decreases monotonically as a decreases, which is consistent with the substantial magnetovolume effects, but for all the lattice parameters studied here these values exceed the Stoner instability

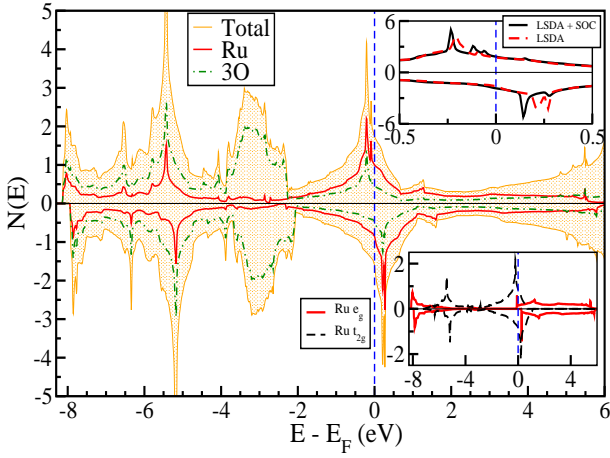


FIG. 4: (Color online) Total and atom-projected DOSs of the FM cubic BaRuO₃ in the full range, including all O 2p and Ru 4d states. In the spin up channel, peaks appear at -0.2 and -0.1 eV. DOS $N(0)$ at E_F is 3.34 states per eV for both spins. *Upper inset*: Expanded view of total DOSs in LSDA and LSDA+SOC between -0.5 and 0.5 eV. *Lower inset*: Ru t_{2g} and e_g orbital-projected DOSs.

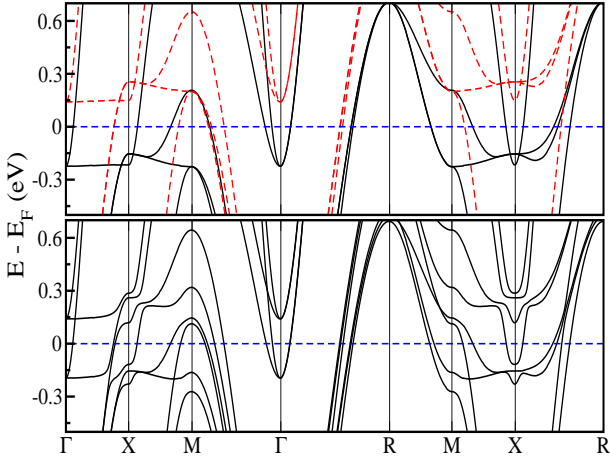


FIG. 5: (Color online) Blowup FM band structure in LSDA (top) and LSDA+SOC (bottom) near E_F in the cubic BaRuO₃. In the top panel, the solid and dashed lines represent the spin up and down characters, respectively. Around the X and M points, the effects of spin-orbit coupling are substantial. The horizontal dashed lines indicate E_F .

criterion $IN(0) \geq 1$.

Electronic structure of FM. Like the FSM results, the LSDA results indicate that the FM state is energetically favored over the nonmagnetic state by 16.4 meV at the optimized lattice parameter. For comparison, from a simple Stoner instability, the energy gain of $Im^2/4$ with $I \approx 0.7$ eV is 175 meV, much larger than the calculated value.

Now, we will address the electronic structure of the FM states. Figure 4 shows the total and atom-projected DOSs, which can be figured out well using the concept

of RuO₆ cluster orbitals.[7] The Ru three t_{2g} states, hybridized with the O six p_π states, produce a bonding manifold at -2 to 1 eV, an antibonding manifold at -6 to -4 eV, and a nonbonding manifold at -4 to -2 eV, as can be visible in the lower inset of Fig. 4. The antibonding and bonding states of Ru two e_g and O three p_σ states lie in the regimes of -8 to -6 eV and 0 to 6 eV, respectively. The exchange splitting of the t_{2g} manifold is about 0.5 eV. In the FM state, the total moment of $1.01 \mu_B$ is decomposed into $0.6 \mu_B$ for Ru and $0.28 \mu_B$ for 3O. (The remnant is in the interstitial regime.)

The enlarged FM band structure of LSDA is given in the top panel of Fig. 5. In this regime, the spin up and down structures are nearly identical, except for a difference in on-site energy of roughly 0.5 eV due to exchange splitting. In the spin up, in addition to a flat band at -0.2 eV along the Γ -X line, which commonly appears in conventional perovskites, two saddle points at the X and M points occur, resulting in vHSs just below E_F . These features may cause the unusual electrical properties observed experimentally.[17]

The band structure of the t_{2g} and p_π cluster in the range of -8 eV to 1 eV was reproduced well using the tight-binding Wannier function technique. We obtained two important parameters: $pd\pi$ hopping $t_\pi = 1.23$ eV and direct oxygen-oxygen hopping $t'_\pi = 0.17$ eV. Compared with the tight-binding parameters of the nonmagnetic CaRuO₃, obtained by Mazin and Singh,[7] t_π is about 10% smaller, but t'_π is about half as large. This is consistent with the 20% smaller bandwidth of the antibonding t_{2g} manifold in BaRuO₃, implying stronger magnetic instability.

Effects of spin-orbit coupling. SOC affects the Fermi surface topology in an isovalent Sr₃Ru₂O₇,[30] though its effects are often negligible in 4d systems. To consider the effects of SOC, we conducted LSDA+SOC calculations. As shown in the upper inset of Fig. 4, the changes in the DOS are relatively small, leading to a tiny orbital moment of $-0.013 \mu_B$ on the Ru ion. However, the mixing of states with other spin channel reduces the net moment by 10 %, bring it closer to the experimentally observed value of $0.8 \mu_B$. [17] The net moment is $0.91 \mu_B$, with local moments of $0.55 \mu_B$ for Ru and $0.26 \mu_B$ for 3O.

An additional remarkable feature is that vHSs move toward E_F in both spin channels. In the spin up channel, vHS at -0.1 eV splits into two peaks, whereas two vHSs merge and move to 0.1 eV in the spin down channel. These features reflect changes in that band structure at the X and M points, as demonstrated in the enlarged band structure in the bottom panel of Fig. 5. The strength of SOC is about 0.1 eV at these points near E_F , but negligible elsewhere. SOC alters the Fermi surface (FS) topology at the X-points, in particular, in the intersecting pipe-like and cube-like FSs (not shown here), which are often observed in conventional perovskites.[31] The open pipe-like surface becomes closed, whereas the cube-like closed one becomes open.

IV. DISCUSSION AND SUMMARY

The Fermi liquid behavior experimentally observed in the low T regime may suggest the presence of correlation effects. Considering that this is a metallic $4d$ system, however, the correlation effects should be weak. In our preliminary calculations using the LDA+U method, applying U to the Ru ion shifts the e_g manifold up and the t_{2g} manifold down, so only the intersecting pipe-like FS disappears. To evaluate the importance of the correlation effects, detailed experimental observations are necessary.

In summary, we investigated the magnetic properties of the ferromagnetic cubic perovskite BaRuO₃, using various first principles calculations: FSM, LSDA, LSDA+SOC, and the Wannier function technique. In the nonmagnetic DOS, the cubic phase has a sharp peak pinning at E_F , yielding $IN(0) \approx 1.2$, beyond the Stoner instability. In the LSDA calculations, a few vHSs appear near E_F in both spin channels, resulting in a strong mag-

netovolume effect of $\Delta M/\Delta a \approx 4.3 \mu_B/\text{\AA}$, significantly higher than that of the Invar system $\mathcal{A}\text{Fe}_2$. The effects of SOC are substantial near E_F around the X and M points and affects the topology of some of FSs, though the strength of SOC is negligible in most regimes. At the optimized volume, the effects of SOC reduce the net moment by 10% from the LSDA value, and it becomes very close to the experimentally observed moment. Our results show that the Stoner instability produces ferromagnetism, and the combined effects of the magnetovolume and SOC determine the magnetic moment. Furthermore, the unusually strong magnetovolume effects may imply atypical transport properties in this FM BaRuO₃, suggesting further questions for experimental research.

Acknowledgments

This research was supported by Korea University.

-
- [1] Y. Maeno, H. Hashimoto, K. Yoshida, S. Nishizaki, T. Fujita, J. G. Bednorz, and F. Lichtenberg, *Nature* **372**, 532 (1994).
 - [2] S.K. Malik, D. C. Kundaliya, and R. D. Kale, *Solid State Commun.* **135**, 166 (2005).
 - [3] A.C.W.P. James and J. B. Goodenough, *J. Solid State Chem.* **74**, 287 (1988).
 - [4] S. A. Grigera, P. Gegenwart, R. A. Borzi, F. Weickert, A. J. Schofield, R. S. Perry, T. Tayama, T. Sakakibara, Y. Maeno, A. G. Green, and A. P. Mackenzie, *Science* **306**, 1154 (2004).
 - [5] L. J. Chang, M. Prager, J. Perßon, J. Walter, E. Jansen, Y. Y. Chen, and J. S. Gardner, *J. Phys.:Condens. Matter* **22**, 076003 (2010).
 - [6] J. M. Longo, P. M. Raccah, and J. B. Goodenough, *J. Appl. Phys.* **39**, 1327 (1968).
 - [7] I. I. Mazin and D. J. Singh, *Phys. Rev. B* **56**, 2556 (1997).
 - [8] J. T. Rijssenbeek, R. Jin, Yu. Zadorozhny, Y. Liu, B. Batlogg, and R. J. Cava, *Phys. Rev. B* **59**, 4561 (1999).
 - [9] A. T. Zayak, X. Huang, J. B. Neaton, and K. M. Rabe, *Phys. Rev. B* **77**, 214410 (2008).
 - [10] J.-S. Zhou, K. Matsubayashi, Y. Uwatoko, C.-Q. Jin, J.-G. Cheng, J. B. Goodenough, Q. Q. Liu, T. Katsura, A. Shatskiy, and E. Ito, *Phys. Rev. Lett.* **101**, 077206 (2008).
 - [11] C. U. Jung, *J. Kor. Phys. Soc.* **58**, 83 (2011).
 - [12] Y. A. Ying, Y. Liu, T. He, and R. J. Cava, *Phys. Rev. B* **84**, 233104 (2011).
 - [13] Y. Shirako, H. Satsukawa, X. X. Wang, J. J. Li, Y. F. Guo, M. Arai, K. Yamaura, M. Yoshida, H. Kojitani, T. Katsumata, Y. Inaguma, K. Hiraki, T. Takahashi, and M. Akaogi, *Phys. Rev. B* **83**, 174411 (2011).
 - [14] L. Klein, J. S. Dodge, C. H. Ahn, J. W. Reiner, L. Mievile, T. H. Geballe, M. R. Beasley, and A. Kapitulnik, *J. Phys.: Condens. Matter* **8**, 10111 (1996).
 - [15] S. A. J. Kimber, J. A. Rodgers, H. Wu, C. A. Murray, D. N. Argyriou, A. N. Fitch, D. I. Khomskii, and J. P. Attfield, *Phys. Rev. Lett.* **102**, 046409 (2009).
 - [16] J.-G. Cheng, J.-S. Zhou, and J. B. Goodenough, *Phys. Rev. B* **80**, 174426 (2009).
 - [17] C.-Q. Jin, J.-S. Zhou, J. B. Goodenough, Q. Q. Liu, J. G. Zhao, L. X. Yang, Y. Yu, R. C. Yu, T. Katsura, A. Shatskiy, and E. Ito, *PNAS* **105**, 7115 (2008).
 - [18] T. Ogawa and H. Sato, *J. Alloys Compd.* **383**, 313 (2004).
 - [19] P. C. Donohue, L. Katz, and R. Ward, *Inorg. Chem.* **4**, 306 (1965).
 - [20] J. M. Longo and J. A. Kafalas, *Mater. Res. Bull.* **3**, 687 (1968).
 - [21] S.-T. Hong and A. W. Sleight, *J. Solid State Chem.* **128**, 251 (1997).
 - [22] J.G. Zhao, L.X. Yang, Y. Yu, F.Y. Li, R.C. Yu, Z. Fang, L.C. Chen, and C.Q. Jin, *J. Solid State Chem.* **180**, 2816 (2007).
 - [23] C. Felser and R. J. Cava, *Phys. Rev. B* **61**, 10005 (2000).
 - [24] Y. Cai, Z.-F. Huang, X. Meng, X. Ming, C. Wang, and G. Chen, *Solid State Sci.* **13**, 350 (2011).
 - [25] D.-M. Han, X.-J. Liu, S.-H. Lv, H.-P. Li, and J. Meng, *Physica B* **405**, 3117 (2010).
 - [26] K. Schwarz and P. Blaha, *Comp. Mat. Sci.* **28**, 259 (2003).
 - [27] K. Schwarz and P. Mohn, *J. Phys. F:Met. Phys.* **14**, L129 (1984).
 - [28] K. Koepnik and H. Eschrig, *Phys. Rev. B* **59**, 1743 (1999).
 - [29] W. Zhang, Ph. D. dissertation, Technical University at Dresden (2007).
 - [30] A. Tamai, M. P. Allan, J. F. Mercure, W. Meevasana, R. Dunkel, D. H. Lu, R. S. Perry, A. P. Mackenzie, D. J. Singh, Z.-X. Shen, and F. Baumberger, *Phys. Rev. Lett.* **101**, 026407 (2008).
 - [31] K.-W. Lee and W. E. Pickett, *Phys. Rev. B* **80**, 125133 (2009).